Nanotechnology, Science and Applications

Dovepress
open access to scientific and medical research

Open Access Full Text Article

ORIGINAL RESEARCH

Photothermal response of CVD synthesized carbon (nano)spheres/aqueous nanofluids for potential application in direct solar absorption collectors: a preliminary investigation

This article was published in the following Dove Press journal:
Nanotechnology, Science and Applications
27 July 2012
Number of times this article has been viewed

Gérrard Eddy Jai Poinern[1]
Sridevi Brundavanam[1]
Monaliben Shah[1]
Iafeta Laava[2]
Derek Fawcett[1]

[1]Murdoch Applied Nanotechnology Research Group, [2]Department of Physics, Energy Studies and Nanotechnology, Murdoch University, Perth, Australia

Abstract: Direct-absorption solar collectors have the potential to offer an unlimited source of renewable energy with minimal environmental impact. Unfortunately, their performance is limited by the absorption efficiency of the working fluid. Nanoparticles of functionalized carbon nanospheres (CNS) have the potential to improve the photothermal properties of the working fluid. CNS are produced by the pyrolysis of acetylene gas in a tube-based electric furnace/chemical vapor deposition apparatus. The reaction takes place at 1000°C in the presence of nitrogen gas without the use of a catalyst. The synthesized CNS were examined and characterized using field-emission scanning electron microscopy, transmission electron microscopy, X-ray diffraction spectroscopy, Raman spectroscopy, thermal gravimetric analysis, and ultraviolet-visible analysis. The CNS powders with a mean particle size of 210 nm were then functionalized using tetraethylammonium hydroxide ($[C_2H_5]_4$ N[OH]) and used to produce a series of aqueous nanofluids with varying mass content. The photothermal response of both the nanofluids and films composed of CNS were investigated under 1000 W/m^2 solar irradiation.

Keywords: solar absorption, carbon nanospheres, nanofluids, photothermal

Introduction

The development of new and efficient energy technologies that can deliver environmentally friendly, practical, and economically sustainable sources of energy is an important factor in tackling global warming and reducing carbon dioxide emissions. Sunlight falling on Earth offers a solution, since the hourly solar flux incident on Earth's surface is greater than the annual human consumption of energy in a year.[1] It is also the largest source of renewable energy, and has been collected, concentrated, and converted into usable forms of energy. However, the major obstacles in optimizing the use of this renewable energy lie in efficiently collecting and converting it into other useful forms of energy. One of the most common methods of collection is through solar thermal collectors, which vary in design for collecting solar radiation and efficiently converting the energy.[2,3] A typical solar thermal collector consists of a black absorber surface, usually plates or tubes that are coated with a spectrally selective material that enhances the absorption of solar energy. The absorber then transfers heat to a working fluid or heat-transfer fluid flowing in tubes encased or attached to the absorber. There are clearly significant advantages to using this type of solar energy collection system: it is potentially 100% renewable, produces no emissions, and greatly reduces the cost of heating the working fluid.

Correspondence: Gérrard Eddy Jai Poinern
Murdoch Applied Nanotechnology Research Group, Department of Physics, Energy Studies and Nanotechnology, School of Engineering and Energy, Murdoch University, Perth, Western Australia 6150, Australia
Tel +61 8 9360 2892
Fax +61 8 9360 6183
Email g.poinern@murdoch.edu.au

However, the efficiency of conventional solar thermal collectors is not only dependent on how effectively the absorber can capture solar energy but also on how effectively heat can be transferred to the working fluid and heat losses from the collector. It is therefore not surprising that there is considerable interest in improving solar energy collection efficiency, which will in turn produce greater heating efficiencies. To significantly reduce the shortcomings of the conventional solar thermal collector, an alternative collector design was proposed in the 1970s. The so-called direct-absorption solar collector has the potential to directly absorb solar energy within the working fluid volume and significantly enhance the heating efficiency of the collector.[2,4] For high-flux applications, the collector consists of a closed-loop heat-exchange circuit that separates the heat-transfer fluid from the potable water circuit. Initially, the solar energy is directly absorbed by working fluid in the absorber panels; the heated working fluid then flows through the piping circuit to the heat exchanger, where it transfers its heat to the potable water circuit. Typical examples of traditional working or heat-transfer fluids such as water, ethylene glycol, water/ethylene glycol mixtures, and oils have been shown to have extremely low adsorptive properties over the solar spectrum ($0.25 < \lambda < 2.5$ μm).[5,6] Therefore, for the direct solar absorption collector to operate at its optimal efficiency, its working fluid must have superior absorption properties over the solar spectrum. Hence the need for seeding the working fluid with suitable particles that can enhance the absorption properties of the base fluid.

Research in the late twentieth century focused on developing black liquids that contained small particle sizes ranging from the millimeter scale down to the micrometer scale that could be used to enhance the absorptive properties of the working fluid. Despite having good absorption properties, many of these particle-seeded fluids or microfluids were abrasive and suffered from particle precipitation and sedimentation, which tended to block tubes, valves, and pumps in the collector piping system.[2,7] Recent developments in nanotechnology have seen the discovery of many new materials with novel properties that are significantly different from their bulk form. The inclusion of nanoparticles in liquids to form stable suspensions has also been investigated, since nanofluids have the potential to significantly improve a number of fluid properties, such as thermal conductivity,[8] heat transfer and transport properties,[9] optical properties,[6] and viscosity.[10] In addition, several researchers have reported that nanofluids have the potential to become an effective working fluid in direct solar thermal collectors.[11–13] For example, a study by Tyagi et al revealed that a nanofluid composed of aluminum nanoparticles and pure water had an increased absorption capacity of 10% compared to a pure-water working fluid in a convention flat-plate solar collector.[14] In a similar study, Han et al were able to demonstrate that nanofluids composed of carbon black particles displayed significant temperature-increase enhancements compared to pure water.[7]

As early as 1985, the discovery of Buckminsterfullerenes, or buckyballs, heralded a renewed interest in new forms of carbonaceous materials. These new carbon nanostructured materials from the C_n family consist of nanotubes (CNTs),[15–17] nanofilaments,[18] nanocapsules,[19] and the recently discovered carbon nanospheres (CNS). CNTs are the blackest materials discovered to date,[20] with excellent thermal and electrical conductivities,[21,22] which makes them highly desirable for a number of applications, such as particle additives to the working fluids of direct solar absorption collectors. The nanosphere form of carbon has been synthesized and studied by a number of research groups worldwide[23–25] due to its novel properties and potential applications. For example, the luminescent and fluorescent properties of carbon quantum dots are being explored as a low-toxicity alternative to metal-based quantum dots.[26,27] Serp et al have classified carbon spheres into three categories: the first contains the C_n family and the well graphitized onion-like structures that have diameters in the range of 2–20 nm; the second contains the less graphitized nanosized spheres that range in diameter from 50 nm to 1 μm; and the final category contains the carbon beads that range in diameter from 1 to several μm.[28]

The properties of CNS are similar to those of graphite or fullerenes. Some of these properties include high temperature stability, a large packing density, and excellent electrical conductivity.[29] These properties make CNS an attractive material for a variety of potential applications, such as lubricating materials, energy-storage devices, supercapacitors, catalyst supports, superconductivity, and special rubber additives.[30,31] Recent studies by Wang et al have demonstrated the possible application of carbon-based graphene nanostructures in computer hardware and nanoelectronic devices.[32] The advantage of replacing copper and other metallic interconnections in micro- and nanoelectronic devices with graphene sheets and carbonaceous nanomaterials is that it will increase performance and overcome the large failure rate in metallic interconnections that has resulted from the trend in miniaturization.[33,34] This paper investigates the potential use of CNS in an aqueous-based nanofluid that has the potential to be used as the working fluid in a direct solar absorption collector.

Many techniques have been used to produce CNS to date: the carbonization of pitch,[25] arc discharge,[35] the pyrolysis

of hydrocarbons such as styrene, toluene, benzene, hexane, and ethene,[36] chemical vapor deposition (CVD),[28,37] the use of micelles,[38] and ultrasonic processing.[39]

The CVD technique is considered to be one of the most effective processes available to produce CNS. In 1996, using a CVD equipped with a catalyst bed composed of mixed-valent oxides and rare earth metals, with methane gas as the carbon source and operating with a reaction temperature of 1100°C, Wang and Kang were able to produce monodispersed CNS.[40] The composite oxide catalyst played a key role in releasing oxygen, which in turn reacted with hydrogen atoms of the methane molecule. The net result of this reaction process was the production of carbon nanostructures. Using a similar technique to Wang and Kang,[40] but using an iron catalyst, Serp et al[28] were able to produce CNS with a size range starting from 10 nm up to a maximum of 300 nm in diameter. Also using a CVD experimental setup operating with reaction temperature range of 650°C–850°C, with a catalyst bed of transitional metal salts supported by kaolin, Miao et al were able to produce CNS and carbon beads ranging in size from 400 nm to 2 μm in diameter.[41]

CVD techniques that produce CNS without the use of catalysts have also been investigated by several researchers. The pyrolysis of both methane and benzene in a hydrogen atmosphere was investigated by Govindaraj et al for the production of CNS.[42] In addition, Qian et al devised a noncatalyzed CVD process that used toluene as the carbon source for producing CNS that ranged in size from 60 nm to 1 μm in diameter.[37] Furthermore, Jin et al have reported the use of a noncatalyzed process for producing CNS that used the direct pyrolysis of a hydrocarbon.[36] The range of hydrocarbons investigated included benzene, ethane, hexane, styrene, and toluene. The size of the CNS produced ranged from 50 nm to 1 μm in diameter.[36]

This study is composed of two parts. In the first part, CNS were synthesized using a single-step CVD process that was capable of producing high yields of CNS without the use of a catalyst bed. In the second part, a two-step method of producing CNS-based nanofluids was adopted. In the first part, the process involved the direct pyrolysis of acetylene gas at a reaction temperature of 1000°C. The use of acetylene as the carbon feedstock made the process more economical than using conventional carbon sources such as hexane and toluene. After pyrolysis, the CNS powder was collected from the deposition sites in the CVD chamber or over water in the collecting chamber, and then examined and characterized using six advanced analysis techniques. These included field-emission scanning electron microscopy (FESEM), transmission electron microscopy (TEM), Raman spectroscopy, X-ray diffraction spectroscopy (XRD), thermogravimetric analysis (TGA), and ultraviolet (UV)-visible analysis. After characterization, the CNS powders were then functionalized using tetraethylammonium hydroxide (TEAH). This was necessary because untreated CNS are extremely hydrophobic, and a reactant was needed to attain suspension stability of the nanofluid. The second part investigates the photothermal response of five CNS-based nanofluids and a CNS base film when exposed to solar irradiation. The CNS film was also examined for its electrical conductivity.

Materials and methods

Chemicals

All chemicals used were of chemical-grade purity, purchased from Sigma-Aldrich (Castle Hill, NSW, Australia) and used without further purification. Milli-Q water (Barnstead Ultrapure Water System D11931; Thermo Scientific, Dubuque, IA) (18.3 MΩ cm^{-1}) was used throughout all synthesis procedures involving aqueous solutions. The reactant/surfactant used in the preparation of the CNS was TEAH ($[C_2H_5]_4N[OH]$).

Synthesis of carbon nanospheres

The pyrolysis of instrument-grade acetylene (C_2H_2) gas in the presence of high-purity nitrogen (N_2) was carried out using a CVD apparatus to synthesize carbon CNS. The CVD setup consisted of a simple electrical furnace equipped with a horizontal quartz tube that was 3.8 cm in diameter and 90 cm in length (Figure 1A). Once the furnace temperature was stabilized at 1000°C, the gases were introduced into the quartz tube of the CVD. The flow rates of both gases were monitored using flow meters (Dwyer Instruments, Michigan City, IN); the acetylene flow rate was 400 standard cubic centimetres per minute (sccm), while the nitrogen flow rate was 1200 sccm. During the pyrolysis process, no metallic catalysts were used, and nitrogen was used as a buffer gas. When both gases entered the quartz tube, the pyrolysis of acetylene immediately took place, and the formation of carbon soot could easily be seen. The soot formed on the inside wall of the quartz tube and also collected on the surface of Milli-Q water in the carbon-collecting chamber.

The difference in weight of the CVD collecting components resulting from carbon deposition over a set period of time enabled the determination of the mass flow rate during the pyrolysis process. Over a series of 5-minute time intervals, a mean carbon deposition rate was found to be 1.990 g

per 5 minutes or 0.398 g per minute. The mass balance indicated that all of the carbon originally contained in the acetylene was deposited onto the collecting components within the CVD. The hydrogen from the acetylene combined with nitrogen to form ammonia (NH_3). Thus, by mass, 92.3% of the acetylene was deposited as carbon in the form of soot during the pyrolysis process. The collected carbon soot was then investigated and characterized using FESEM, TEM, XRD, Raman spectroscopy, TGA, and UV-visible analysis.

Characterization of carbon nanospheres

The particle size and structural and morphological features of the carbon soot were investigated using both FESEM and TEM. The morphological features of the soot were investigated using a high resolution FESEM (1555 VP-FESEM; Zeiss, Oberkochen, Germany) at 3 kV with a 30-µm aperture operating under a pressure of 1×10^{-10} Torr, (Figure 2). TEM scans were taken using a Philips (Amsterdam, Netherlands) CM100 Twin TEM operating at 1×10^{-8} Torr pressure and a voltage of 80 kV. Images from both techniques were also used to graphically determine the mean CNS diameter.

The XRD spectra were recorded using a Siemens (Berlin, Germany) D500 series diffractometer (Cu K_α = 1.5406 Å radiation source) operating at 40 kV and 30 mA. The diffraction patterns were collected at room temperature over the 2θ range from 20°C to 60°C with an incremental step size of 0.04°. The acquisition time was 2.0 seconds. The Raman spectra of the samples were recorded using a LabRAM model 2B dispersive Raman spectrophotometer (Horiba, Kyoto, Japan) that was equipped with a 2-mW helium–neon (λ = 632 nm) laser. All spectra were collected between 4000 cm^{-1} and 125 cm^{-1} using a diffraction grating consisting of 600 lines per millimeter.

TGA was used to investigate the thermal stability of the CNS using an SDT 2960 (TA Instruments, New Castle, DE). Initially, two 8-mg carbon soot samples were prepared; the first sample was used in a high-purity argon atmosphere, and the second sample was used in normal atmospheric air. The TGA procedure determined the start and completion of the oxidation process of each sample and the respective atmosphere in turn as the temperature was increased, (heating rate of 10°C/minute) from room temperature (24°C) to a maximum temperature of 900°C, (see Figure 3). The UV-visible response of the carbon soot was examined by first dissolving a small amount of CNS in ethanol. The mixture was then passed through a 0.22 µm Whatman Millipore syringe filter, and the resulting filtrate was examined using a Varian (Palo Alto, CA) Cary 50 series UV-visible spectrophotometer version 3, over a spectral range of 200–800 nm, with a 1-nm resolution over 1 hour using a scan rate of 400 nm per sec at a room temperature of 24°C.

Functionalization of carbon nanospheres and synthesis of nanofluids

The synthesized CNS powders were found to be extremely hydrophobic and needed to be functionalized before being dispersed in Milli-Q water (see Figure 4B insert). Functionalization consisted of adding 1–2 mL of 20% TEAH to a specific mass of CNS powder in a mortar. The range of CNS sample masses functionalized was 0.005, 0.010, 0.020, 0.030, and 0.040 g. Each individual sample was then ground for 15 minutes to produce a smooth paste using a pestle and mortar. The paste was then added to a small vial containing a solution of 10 mL of 20% TEAH and 90 mL of Milli-Q water. The mixture was then sonicated for 1 hour using an ultrasonic processor (UP50H, 100% amplitude, 50 W, 30 kHz, MS7 Sonotrode [7 mm diameter, 80 mm length]; Hielscher Ultrasonics, Teltow, Germany) to disperse the CNS.

Photothermal response of a CNS-based film in air

The effectiveness of using a CNS film for temperature enhancement of a substrate surface exposed to solar irradiation was investigated. A functionalized CNS paste was made by mixing 1–2 ml of 20% TEAH with 0.05 g CNS powder in a mortar. The mixture was then ground for 15 minutes to produce a smooth paste using a pestle and mortar. Two 15-mm squares of Parafilm M (SPI Supplies, West Chester, PA) sealing film were cut. The first was untreated and used as the control. The second was coated with a thin layer of CNS paste that was evenly spread over the upper surface. The film was then allowed to naturally air-dry. Both film samples were then laid on a standard laboratory glass slide for support and handling. The slide was then placed into a specifically designed light box fitted with a solar light source (1000 W/m^2). Both films were initially photographed using a thermal imager (Ti25; Fluke, Everett, WA) and then irradiated for 160 seconds. At the end of this time, both films were again photographed using the thermal imager. The photographic data was then processed and used to produce a set of before-and-after thermal images (see Figure 5A).

Photothermal response of nanofluids

The photothermal response of the nanofluids was carried out in a specifically designed light box fitted with a solar light source (1000 W/m^2). The nanofluids were sealed in

glass vials, all filled to the same level to ensure the same thermal transfer area. The temperatures of each nanofluid sample were monitored using a QM-1600 meter (Digitech, Hounslow, UK) with the thermocouple inserted into the fluid. Three sets of temperature measurements were carried out and recorded in real time, with the average value being used. The average atmospheric temperature was 28°C.

Electrical conductivity measurements

Thin films with a mean thickness of 0.3 mm composed of functionalized CNS were examined for their electrical conductivity. The functionalized CNS paste was made by mixing 1–2 mL of 20% TEAH with 0.05 g CNS powder in a mortar. The mixture was then ground for 15 minutes using a pestle and mortar to produce a smooth paste. Then three 15-mm squares of Parafilm M sealing film were cut; these were used as backing support for the CNS film. The Parafilm M films were then coated with a thin layer of CNS paste that was evenly spread over the upper surface. The film was then allowed to naturally air-dry. The electrical conductivity characteristics of all three CNS films were carried out using a power supply (Escort dual tracking, model 3030TD; Microtek Instruments, Chennai, India) as the voltage source. The current and voltage measurements were taken using two digital multimeters (True RMS Digital Multimeter model 506; Protek, Morwood, NJ). The voltmeter probes were positioned 1 cm apart on the surface of the CNS film. Three sets of measurements were carried out on each film, and average values from all three sets of film measurements were used to produce a representative current–voltage curve for the film.

Results and discussion

The structural and morphological features of the CNS produced from the pyrolysis of acetylene were examined using both TEM (Figure 1B) and FESEM (Figure 2). Figure 1 presents TEM images of the carbon soot particles that were collected directly from the collecting components within the CVD. The FESEM images (Figure 2) reveal that the untreated soot, in bulk, appears black and is composed of nanosized carbon spheres. The sphere diameters range in size from 100 nm to 400 nm. This spherical particle morphology was confirmed by the TEM analysis. The images reveal that the CNS are consistently spherical in shape and range in size from 100 nm to 500 nm in diameter. Graphical analysis of both FESEM and TEM images revealed that the mean particle size of the CNS was 210 nm. The images of both FESEM and TEM also clearly demonstrate that a metallic catalyst was not needed during the pyrolysis of acetylene to form CNS.

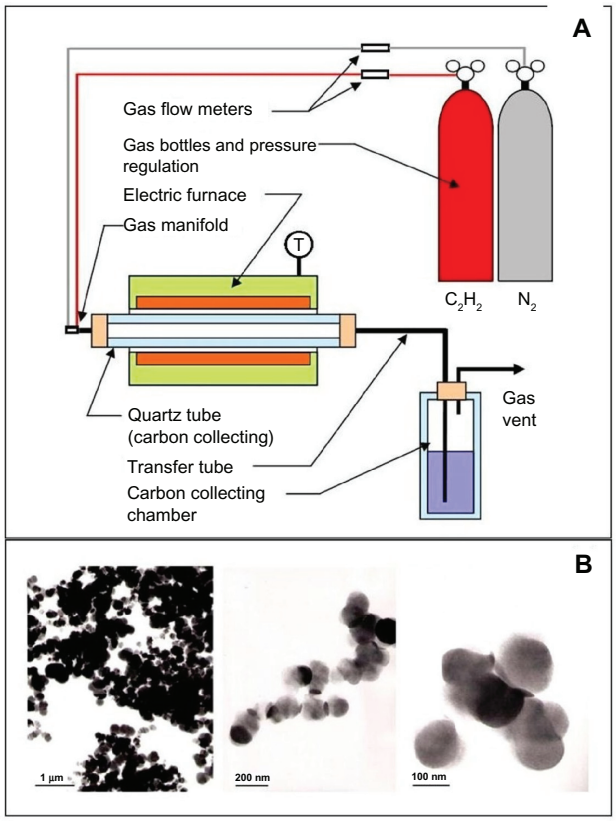

Figure 1 (**A**) Schematic of the chemical vapor deposition equipment; (**B**) transmission electron microscopy images of carbon nanospheres produced by the pyrolysis of acetylene gas taken at three magnifications (**left** 1 µm, **middle** 200 nm, and **right** 100 nm).

The bonding and thermal stability of the produced CNS was investigated using both Raman spectroscopy and XRD. The Raman spectrum presented in Figure 3A reveals two prominent peaks, the first located at 1325 cm^{-1} and the second at 1583 cm^{-1}. The first peak represents the D band, which results from defects and the disordered nature of the carbon soot, while the second peak results from the graphitization of the carbon soot (stretching mode of the carbon–carbon bonds). The peak intensity ratio of the D and G bands (I_D/I_G) is commonly used to describe the degree of graphitization of a carbon material.[43,44] A recent study involving the noncatalytic pyrolysis of toluene to synthesize CNS by Qian et al produced a peak intensity ratio of 0.84,[37] while Xu et al[23] reported a value of 1.15 for pyrolyzing a mixture of C_2Cl_4 and $Fe(CH_5)_2$.[45] This investigation found a peak intensity ratio value of 1.14; this value indicates that the CNS produced in this work have a lower degree of graphitization and the presence of disordered carbon.[29,41]

To confirm the degree of graphitization that has taken place in producing the CNS, an XRD study was undertaken. The results of the XRD study are presented in Figure 3B;

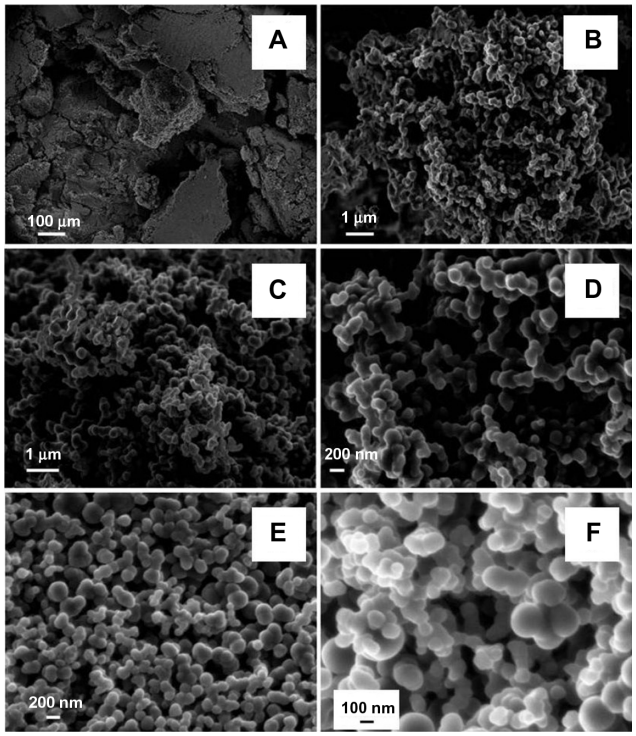

Figure 2 (**A**–**F**) Field-emission scanning electron microscopy images of carbon nanospheres produced by the pyrolysis of acetylene gas taken at various magnifications ranging from 100 µm down to 100 nm.

inspection of the XRD pattern reveals two dominant peaks, the first occurring at a 2θ angle of 24.96° and 45.08°. These angles correspond to the (002) and (100) graphitic planes, respectively. Figure 4B also reveals a broadening in the XRD peaks, suggesting that there is some amorphous carbon structure present with a lower degree of graphitization. These results are similar to those reported by Jin et al, who produced CNS from a variety of hydrocarbons.[36]

TGA was used to investigate the thermal stability of the CNS; the results are presented graphically in Figure 3A. The initial thermal stability investigation was carried out in an Argon atmosphere (curve 1) from room temperature to 900°C. Over this temperature range, a 4.619% weight loss was detected in the sample, which was believed to be the result of the amorphous carbon and trapped gases escaping from the sample. The TGA result for argon indicates that the CNS retained their spherical morphology and structural stability at temperatures up to 900°C in an inert atmosphere. This behavior is similar to the results obtained by Jin et al in a similar study.[36] In the second part of the experiment, the thermal stability of the CNS in air (curve 2) was investigated. This was done because the CNS are known to be sensitive to oxidation. From Figure 3A, it is evident that the sample was stable below 500°C, but at higher temperatures there was a rapid onset of oxidation. Just above 500°C, the oxidation process began and rapidly increased until a sharp declining slope developed at 562.12°C, indicating the onset of a rapid oxidation rate. The steepness of this slope indicates that there are a large number of lattice defects in the structure of the CNS that enable oxygen to travel into the structure and facilitate a high oxidation rate. The oxidation process continued until all the carbon soot was completely oxidized, and the reaction abruptly ended at 658.19°C.

UV-visible analysis was used to investigate the fluorescent properties of the CNS produced in this work. The ultraviolet response of oxidized carbon nanoparticles formed in candle soot was first demonstrated by Liu et al.[27] In their study, they found that the fluorescent properties of the candle soot were dependent upon the size of the carbon nanoparticles formed. A similar technique was used in this work to investigate the UV-visible response of the CNS. In general, carbon soot is highly hydrophobic; however, the CNS produced in this study were able to be dissolved in alcoholic solutions.[23] A small quantity of CNS were dissolved in ethanol, filtered using a 0.22-µm syringe filter and then submitted to UV-visible analysis. The absorbance peaks in the UV-visible spectrum are presented in Figure 3B. The preliminary optical results indicate that the CNS produced by the pyrolysis of acetylene show absorbance peaks, which could relate to the different CNS sizes. Furthermore, under UV irradiation, the CNS in ethanol are fluorescent, as seen in the Figure 3B insert. This preliminary study clearly indicates that further investigation is needed.

Nanofluid stability is influenced by particle properties such as morphology and surface chemistry and the chemistry of the base fluid. The CNS synthesized in this work have a surface chemistry that makes them extremely hydrophobic (see Figure 4B insert, i). Therefore, it was necessary to functionalize the surface of the CNS using TEAH, which effectively modified the surface chemistry of the CNS. The fictionalization process effectively increased the wettability of the CNS surface, which allowed easier dispersion of the CNS into the Milli-Q water, hence forming the CNS-based aqueous nanofluid suspension (see Figure 4B insert, ii). The CNS-based aqueous nanofluid suspensions were stable for periods ranging from 2 to 3 weeks. After 2 weeks of standing in a glass vial under standard laboratory conditions, CNS particle precipitation could be observed. And by the end of the third week, sedimentation could be easily seen in the bottom of the vial. Further investigation is needed to improve the long-term stability of the CNS nanofluids for periods greater than 2 weeks, when the nanofluid is left standing for extended periods.

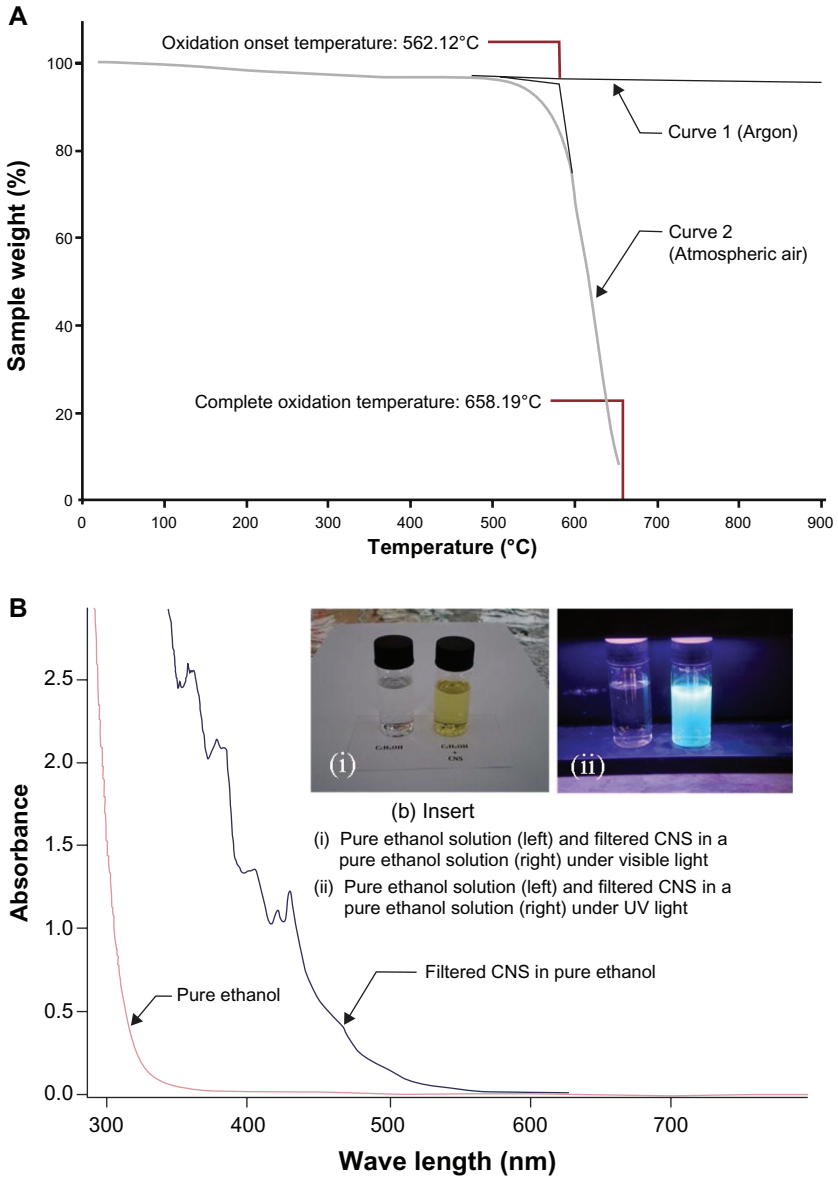

Figure 3 (**A**) Thermogravimetric analysis of carbon nanospheres (CNS) carried out in both argon and atmospheric air from room temperature up to 900°C; (**B**) ultraviolet (UV)-visible spectrum of pure ethanol and filtered CNS dispersed in pure ethanol.

When a thin CNS layer film deposited on a Parafilm M film was exposed to 1000 W/m^2 of solar irradiation, there was a significant photothermal response. After 30 seconds, the temperature of CNS-coated film was 4.5°C higher than the uncoated Parafilm M film, and after 160 seconds the temperature difference was 6.2°C. Thermal images of the CNS-coated and uncoated films are presented in Figure 5A. The complete thermal data for the 160-second test period are presented; the graphical plots reveal that there was a significant temperature difference throughout the test period. The data confirm that the CNS coating was able to provide a significant temperature enhancement to the Parafilm M film. In addition, the results of electrical conductivity measurements revealed that the current–voltage characteristics of the TEAH-functionalized CNS films were linear (ohmic behavior) over the experimental range examined (see Figure 6B). The slope of the line fit indicates that the resistance of the CNS films was relatively high, with a mean value of 920 ± 30 kΩ between the test probes (1 cm spacing).

A similar temperature-enhancement trend was also seen with the inclusion of CNS in an aqueous-based nanofluid. The base solution was composed of a solution of 10 mL 20% TEAH and 90 mL Milli-Q water. The presence of TEAH in the base solution had no significant photothermal response when compared to the pure Milli-Q water control solution; therefore, the photothermal response seen in all

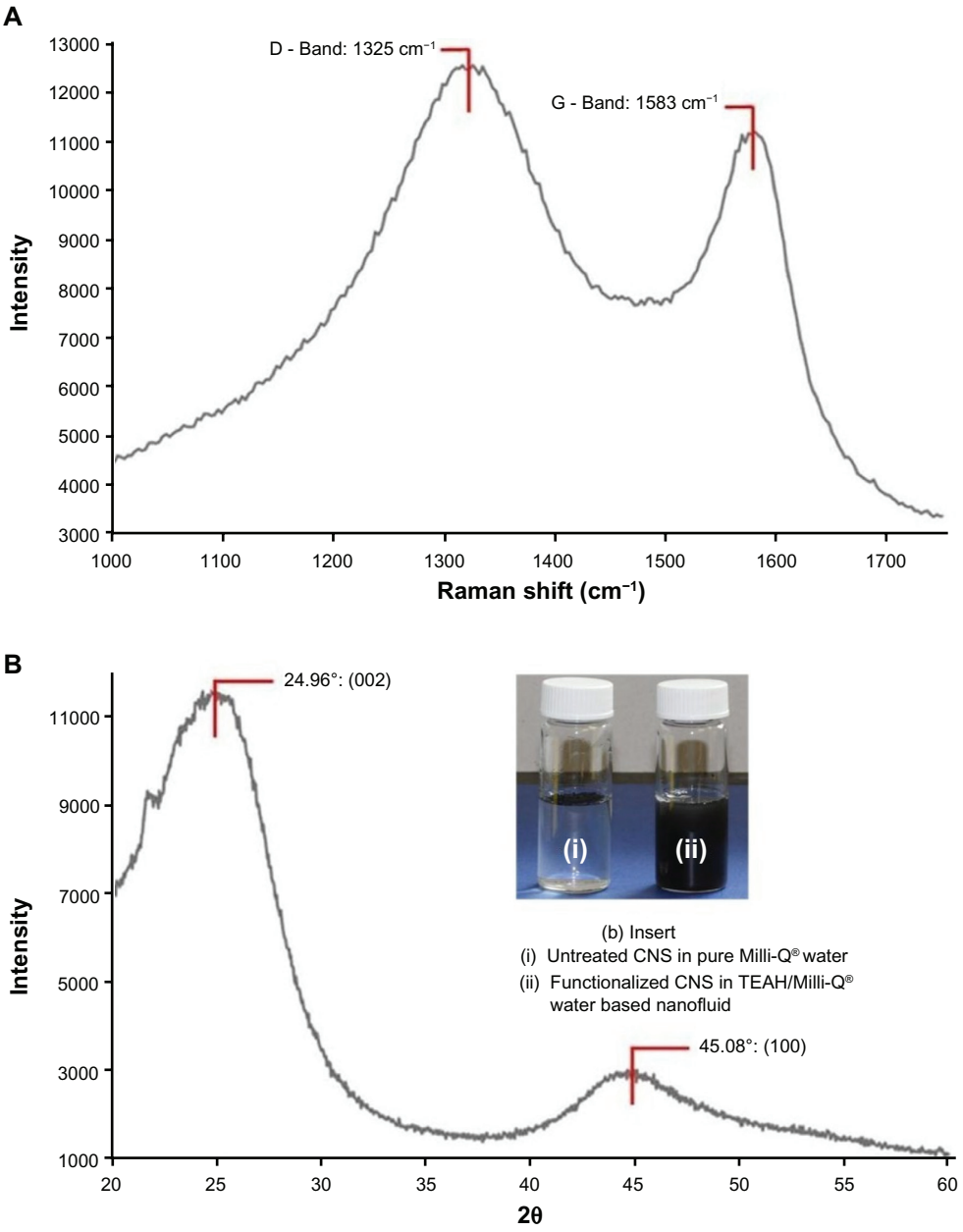

Figure 4 (**A**) Raman spectrum and (**B**) X-ray diffraction spectroscopy pattern of carbon nanospheres (CNS) produced by the pyrolysis of acetylene gas; insert (b) untreated CNS in Milli-Q water and functionalized CNS in tetraethylammonium hydroxide (TEAH)/Milli-Q water-based nanofluid.

CNS nanofluids was the result of the CNS present. This can be seen in Figure 5B, in which increasing amounts of CNS in the base solution produce a greater photothermal response. In the case of the nanofluid with the smallest mass of CNS present (0.005 g); the temperature enhancement after 60 minutes was 3.5°C, while the nanofluid with the largest mass of CNS (0.04 g) had a temperature enhancement of 8.1°C for the same period of time (see Figure 6A). This result clearly indicates increasing CNS mass content in the nanofluid significantly improves the photothermal properties in the experimental range.

However, a similar study by Han et al using carbon black nanofluids found that the temperature enhancement of a 7.7-vol% carbon black nanofluid was similar to a 6.6-vol% sample, thus indicating that the photothermal properties did not increase significantly above the 6.6-vol% sample.[7] The 7.7-vol% carbon black nanofluid was found to produce a 7.2°C temperature enhancement compared to pure water. This is similar to the 8.1°C temperature enhancement of the 0.04-g CNS nanofluid, the only major difference being in the type of carbon and its content. In terms of volume fraction, the 0.04-vol% (0.04 g) used in this study was significantly less than the values used

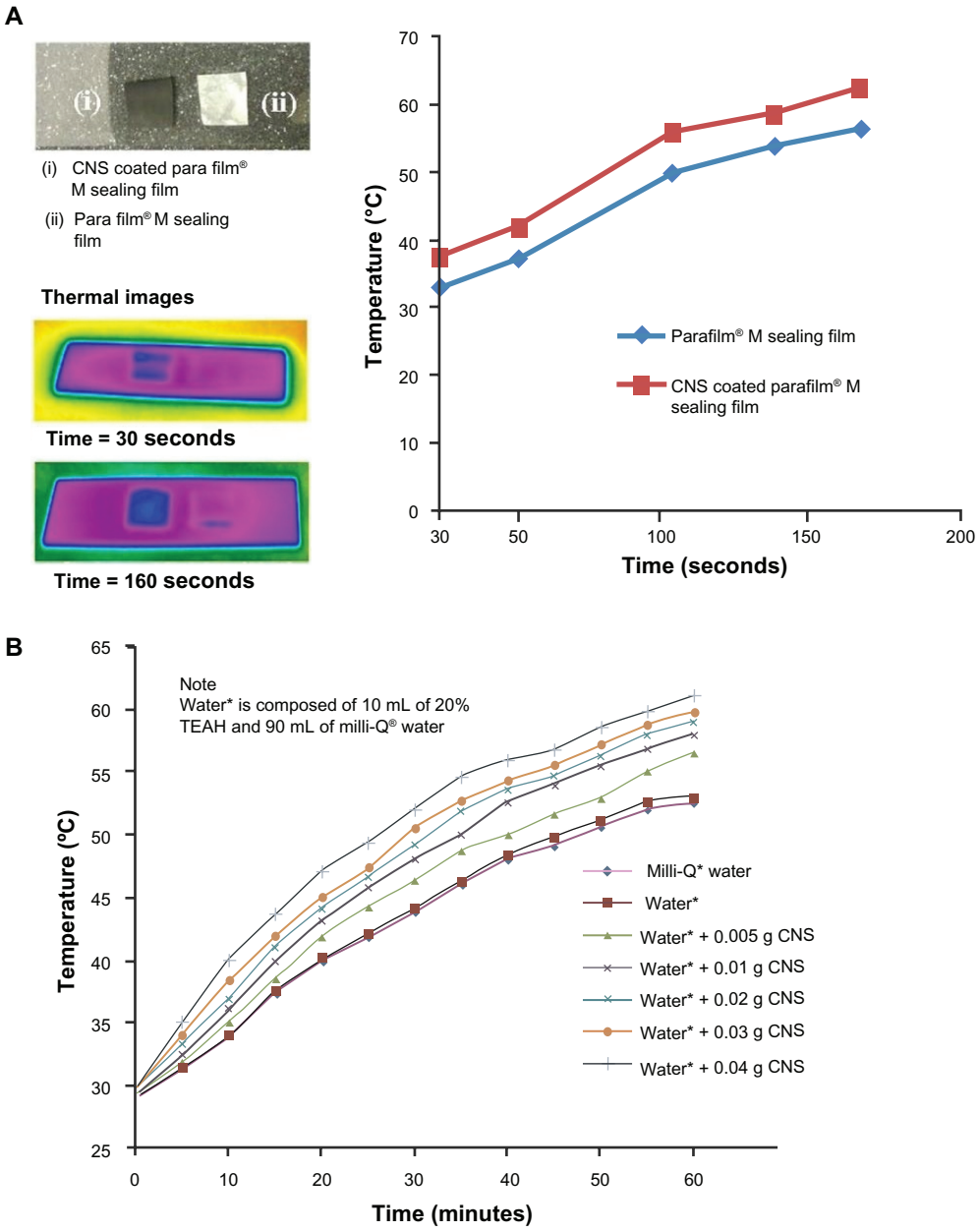

Figure 5 (**A**) Photothermal response of a carbon nanosphere (CNS)-coated film; (**B**) photothermal response of five CNS-based nanofluids of varying CNS mass content.
Abbreviation: TEAH, tetraethylammonium hydroxide.

by Han et al.[7] In addition, the CNS functionalized with TEAH appear to have enhanced photothermal properties compared to carbon black when we consider the low volume fractions being used in this work. Han et al also pointed out that the temperature enhancements of their carbon black nanofluids were higher than those of Mu et al's TiO_2/water, SiO_2/water, and ZrC/water nanofluids (<1 wt%).[7,46] The superior photothermal response of the carbon black nanofluids is believed to be due to the high concentration and good solar absorption of carbon black present in the water based fluid compared to the metallic nanoparticles used by Mu et al.[46] The CNS used in this work also display the superior solar absorption properties of carbon black, but with much lower volume fractions. The lower fractions of CNS used this work make them highly suitable for incorporation into water based working fluids within a conventional pumping system, since unlike larger micrometer-sized particles, the nanosized CNS will have few detrimental effects, such as increased fluid friction, sedimentation, and blockages.

Conclusion

CNS were produced via the noncatalyzed pyrolysis of acetylene gas at 1000°C in the presence of nitrogen gas in a simple

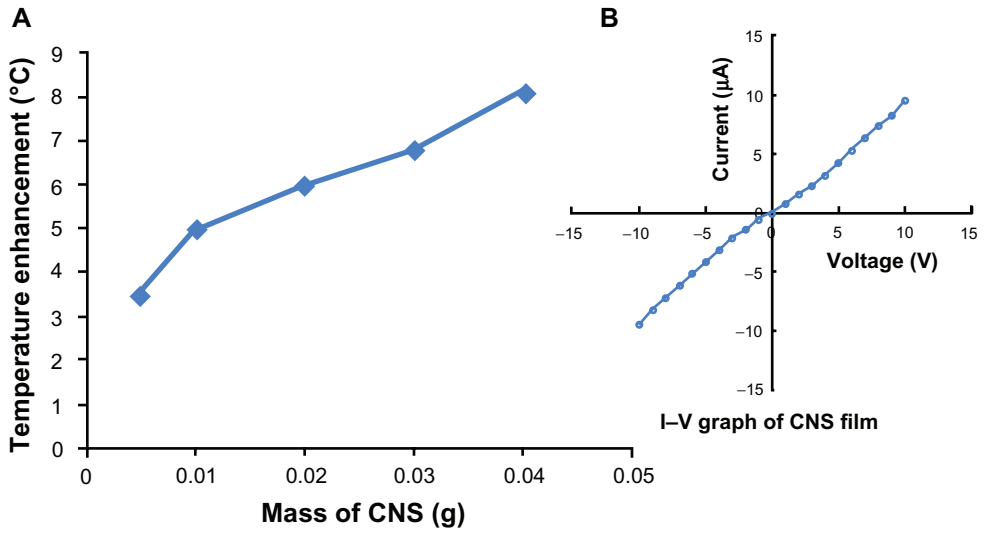

Figure 6 (**A**) Temperature enhancement produced by increasing mass content of carbon nanospheres (CNS) in the nanofluids; (**B**) electrical conductivity of a typical tetraethylammonium hydroxide–functionalized CNS-coated Parafilm M film.

electric furnace–based CVD apparatus. The resultant carbon soot contained CNS that ranged in size from 100 nm to 500 nm in diameter. Raman spectroscopy, XRD, and TGA analysis indicated a lower degree of graphitization in the CNS, which produced stable spherical structures with a mean particle size of 210 nm. The preliminary UV-visible analysis of filtered CNS dispersed in ethanol revealed some interesting features that will need further investigation. In addition, a detailed study is needed to investigate the effect of different reaction conditions on the size, structure, and morphology of CNS being formed during pyrolysis. The results of this further study would provide information needed to effectively control the formation mechanisms operating during the pyrolysis process. Refinement of the formation mechanism would allow fine tuning of the CNS size, structure, and morphology.

The CNS were then functionalized using TEAH before being dispersed in Milli-Q water to form nanofluids of varying CNS mass content. All of the CNS nanofluids had favorable photothermal responses to solar irradiation over the exposure period. The largest CNS mass content (0.04 g) nanofluid had the largest temperature enhancement of 8.1°C, which clearly demonstrates efficient absorption capabilities of the CNS nanofluids towards solar irradiation compared to Milli-Q water. The results indicate that functionalized CNS nanofluids have the potential to effectively improve the solar absorption capabilities of direct-absorption solar collectors.

Acknowledgments

The authors would like to thank Mr Ravi Krishna Brundavanam for his valuable assistance during this project and Mr Ken Seymour for his assistance in the TGA analysis. The authors would also like to thank Dr Sinsa Djordjevic for the thermal imaging analysis and Dr Zhong-Tao Jiang for his helpful discussions. The authors acknowledge the financial support provided by the West Australian Nanochemistry Research Institute (WANRI) for this project.

Disclosure

The authors report no conflict of interest in this work.

References

1. Lewis NS. Toward cost-effective solar energy use. *Science*. 2007; 315(5813):798–801.
2. Minardi JE, Chuang HN. Performance of a black liquid flat-plate solar collector. *Sol Energy*. 1975;17:179–183.
3. Kalogirou SA. Solar thermal collectors and applications. *Prog Energy Combust Sci*. 2004;30:231–295.
4. Arai N, Itaya N, Hasatani M. Development of a volume heat-trap type solar collector using a fine-particle semitransparent liquid suspension (FPSS) as heat vehicle and heat storage medium: unsteady, one dimensional heat transfer in a horizontal FPSS layer heated by thermal radiation. *Sol Energy*. 1984;32(1):49–56.
5. Taylor RA, Phelan PE, Otanicar TP, Adrian R, Parsher R. Nanofluid optical property characterisation: towards efficient direct absorption solar collectors. *Nanoscale Res Lett*. 2011;6(225):1–11.
6. Otanicar TP, Phelan PE, Golden JS. Optical properties of liquids for direct absorption solar thermal energy systems. *Sol Energy*. 2009;83(7):969–977.
7. Han D, Meng Z, Wu D, Zhang C, Zhu H. Thermal properties of carbon black aqueous nanofluids for solar absorption. *Nanoscale Res Lett*. 2011;6(457):1–7.
8. Wang XQ, Majumdar AS. Heat transfer characteristics of nanofluids: a review. *J Therm Sci*. 2007;46:1–19.
9. Wang XQ, Mujumdar AS. A review on nanofluids – part II: experiments and applications. *Braz J Chem Eng*. 2008;25(4):631–648.
10. Prasher R, Song D, Wang J, Phelan P. Measurements of nanofluid viscosity and its implications for thermal applications. *Appl Phys Lett*. 2006;89(13):133108–133110.

11. Mao LB, Zhang RY, Ke XF. The photo-thermal properties of copper nanofluids. *J Guangdong Univ Technol*. 2008;25:13–17.
12. Otanicar TP, Phelan PE, Prasher RS, Rosengarten G, Taylor RA. Nanofluid based direct absorption solar collector. *J Renew Sustain Energy*. 2010;2(3):033102.
13. Taylor RA, Phelan PE, Otanicar TP, et al. Application of nanofluids in high flux solar collectors. *J Renew Sustain Energy*. 2011;3:023104.
14. Tyagi H, Phelan PE, Prasher R. Predicted efficiency of a low-temperature nanofluid based direct absorption solar collector. *J Sol Energy Eng*. 2009;131(4):041004.
15. Kroto HW, Heath JR, O'Brien SC, Curl RF, Smalley RE. C60: Buckminister fullerene. *Nature*. 1985;318:162–163.
16. Iijima S. Helical micro-tubules of graphitic carbon. *Nature*. 1991;354: 56–58.
17. Poinern GEJ, Parsonage D, Issa TB, Ghosh MK, Paling E, Singh P. Preparation, characterisation and AS(V) adsorption behaviour of CNT-ferrihydrite composites. *Int J Eng Sci Technol*. 2010;2(8):13–24.
18. Lee SY, Yamada M, Miyake M. Synthesis of carbon nano-tubes and carbon nano-filaments over palladium supported catalysts. *Sci Technol Adv Mat*. 2005;6(5):420–426.
19. Sano N, Akazawa H, Kikuchi T, Kanki T. Separated synthesis of iron-included carbon nanocapsules and nanotubes by pyrolysis of ferrocene in pure hydrogen. *Carbon*. 2003;41(11):2159–2162.
20. Yang ZP, Ci L, Bur JA, et al. Experimental observation of an extremely dark material made by a low density nano-tube array. *Nano Lett*. 2008;8(2):446–451.
21. Singer P. CNTs an attractive alternative for interconnects (carbon nano-tubes). *Semicond Int*. 2007;30(5):26–33.
22. Poncharal P, Berger C, Yi Y, Wang ZL, de Heer Walt A. Room temperature ballistic conduction in carbon nanotubes. *J Phys Chem B*. 2002;106(47):12104–12118.
23. Xu L, Zhang W, Yang Q, et al. A novel route to hollow and solid carbon spheres. *Carbon*. 2005;43(5):1090–1092.
24. Wang Q, Li H, Chen L, Huang X. Mono-dispersed hard carbon spherules with uniform nanopores. *Carbon*. 2001;39(14):2211–2214.
25. Lee SI, Yoon SH, Park CW, Korai Y, Mochida I. Preparation of microporous carbon nanospheres. *Carbon*. 2002;411:1645–1687.
26. Sun YP, Zhou B, Lin Y, et al. Quantum-sized carbon dots for bright and colourful photoluminescence. *J Am Chem Soc*. 2006;128(24): 7756–7757.
27. Liu H, Ye T, Mao C. Fluorescent carbon nanoparticles derived from candle soot. *Angew Chem Int Ed Engl*. 2007;119:6593–6595.
28. Serp PH, Feurer R, Kalck PH, et al. A chemical vapour deposition process for the production of carbon nanospheres. *Carbon*. 2001;39(4): 615–618.
29. Yuan D, Chen J, Zeng J, et al. Preparation of monodisperse carbon nanospheres for electrochemical capacitors. *Electrochem Commun*. 2008;10(7):1067–1070.
30. Yang R, Qiu X, Zhang H, et al. Mono-dispersed hard carbon spherules as a catalyst support for the electro-oxidation of methanol. *Carbon*. 2005;43(1):11–16.
31. Wang Y, Su F, Wood CD, Lee JY, Zhao XS. Preparation and characterization of carbon nanospheres as anode materials in lithium-ion secondary batteries. *Ind Eng Chem Res*. 2008;47(7):2294–2300.
32. Wang X, Ouyang Y, Li X, et al. Room-temperature all-semiconducting sub-10-nm graphene nanoribbon field-effect transistors. *Phys Rev Lett*. 2008;100(20):206803.
33. Novoselov KS, Geim AK, Morozov SV, et al. Electric field effect in atomically thin carbon films. *Science*. 2004;306(5696):666–669.
34. Coiffic JC, Le Poche H, Mariolle D, et al. Towards the integration of a single carbon nanofiber as via interconnect. *Microelectron Eng*. 2008;85(10):1971–1974.
35. Qiao WM, Song Y, Lim SY, et al. Carbon nanospheres produced in an arc-discharge process. *Carbon*. 2006;44(1):187–190.
36. Jin YZ, Gao C, Hsu WK, et al. Large-scale synthesis and characterization of carbon spheres prepared by direct pyrolysis of hydrocarbons. *Carbon*. 2005;43(9):1944–1953.
37. Qian HS, Han FM, Zhang B, et al. Non-catalytic CVD preparation of carbon spheres with a specific size. *Carbon*. 2004;42(4):761–766.
38. Kim BJ, Chang JY. Preparation of carbon nanospheres from diblock copolymer micelles with cores containing curable acetylenic groups. *Macromolecules*. 2006;39(1):90–94.
39. Wang Z, Yu L, Zhang W, et al. Carbon spheres synthesized by ultrasonic treatment. *Phys Lett A*. 2003;307(4):249–252.
40. Wang ZL, Kang ZC. Pairing of pentagonal and heptagonal carbon rings in the growth of nanosize carbon spheres synthesized by a mixed-valent oxide-catalytic carbonization process. *J Phys Chem*. 1996;100(45):17725–17731.
41. Miao JY, Hwang DW, Narasimhulu KV, et al. Synthesis and properties of carbon nanospheres grown by CVD using kaolin supported transition metal catalysts. *Carbon*. 2004;42(4):813–822.
42. Govindaraj A, Sen R, Nagaraju BV, Rao CNR. Carbon nanospheres and tubules obtained by the pyrolysis of hydrocarbons. *Philos Mag Lett*. 1997;76(5):363–367.
43. Tessonnier JP, Rosenthal D, Hasen TW, et al. Analysis of the structure and chemical properties of some commercial carbon nanostructures. *Carbon*. 2009;47(7):1779–1798.
44. Sadezky A, Muckenhuber H, Grothe H, Niessner R, Poschl U. Raman micro-spectroscopy of soot and related carbonaceous materials: spectral analysis and structural information. *Carbon*. 2005;43(8):1731–1742.
45. Dimovski S, Nikitin A, Ye H, Gogotsi Y. Synthesis of graphite by chlorination of iron carbide at moderate temperatures. *J Mater Chem*. 2004;14:238–243.
46. Mu LJ, Zhu QZ, Si LL. Radiative properties of nanofluids and performance of a direct solar absorber using nanofluids. 2nd ASME Micro/Nanoscale Heat and Mass Transfer International Conference; December 18–21, 2009; Shanghai, China.